Chapter 5

Modeling, System Identification, and Control of Electromagnetic Actuators

Alexandru Forrai

Additional information is available at the end of the chapter

http://dx.doi.org/10.5772/intechopen.75088

Abstract

This chapter is dedicated to modeling, system identification, and control of electromagnetic actuators with the main focus on the actuators used in magnetic levitation, in fuel injection systems, and in variable valve timing (VVT). These actuators have a simple structure, good reliability, and low manufacturing costs. However, from control viewpoint, they are nonlinear systems and are open-loop unstable. Therefore, mathematical modeling, system identification-based parameter estimation, and control strategies are presented, when the moving armature is controlled around an equilibrium position or is controlled between the two extreme positions of the armature.

Keywords: electromagnetic actuator, modeling, identification, gain scheduled control

1. Introduction

Electromagnetic actuators are widely used in the industry, and they transform the electric energy into linear motion. From the large variety of applications, in this chapter we are going to focus on:

- Magnetic levitation
- Fuel injection systems and variable valve timing actuators used in internal combustion engines

These applications are relevant from control point of view: in the first case, the moving armature is controlled around an equilibrium position; in the second case, the armature might go under control between the two extreme positions—armature open and armature close.

Nevertheless, magnetic levitation—in particular a magnetically levitated train—is a good example, where closed-loop control plays a key role, since the open-loop system is unstable [1]. The system can be linearized around an operating point, and a linear controller can be designed.

Furthermore, magnetic bearings and their control are from a long time the focus of control system design community. Feedback linearization and asymptotically exact linearization of an active magnetic bearing are presented in [2, 3]. Advanced control strategies are discussed in detail in [4, 5].

Therefore, it makes sense to develop high-accuracy mathematical models, to investigate methods for parameter identification, and finally to apply control strategies to improve performance and reliability of the system.

We will discuss these topics in the next sections, but before that let us focus on applications, where electromagnetic actuators are widely used.

1.1. Magnetic levitation

Magnetic bearings in combination with high-speed electric motors are used across many industries, from oil and gas industry to electric power generation industry (i.e., high-speed electric generators) and from the semiconductor industry to nuclear industry, etc.

The main structure of the magnetic bearing is shown in **Figure 1** (reproduced from [6]).

Another well-known application of the magnetic levitation is the magnetically levitated high-speed train (Maglev; see **Figure 1**), having speeds over 500 [km/h] [7, 8].

1.2. Fuel injection and variable valve timing (VVT)

The main purpose of the fuel injection system is to deliver fuel to the cylinders. However, how that fuel is delivered is that it makes the difference in engine performance, emissions, and noise characteristics.

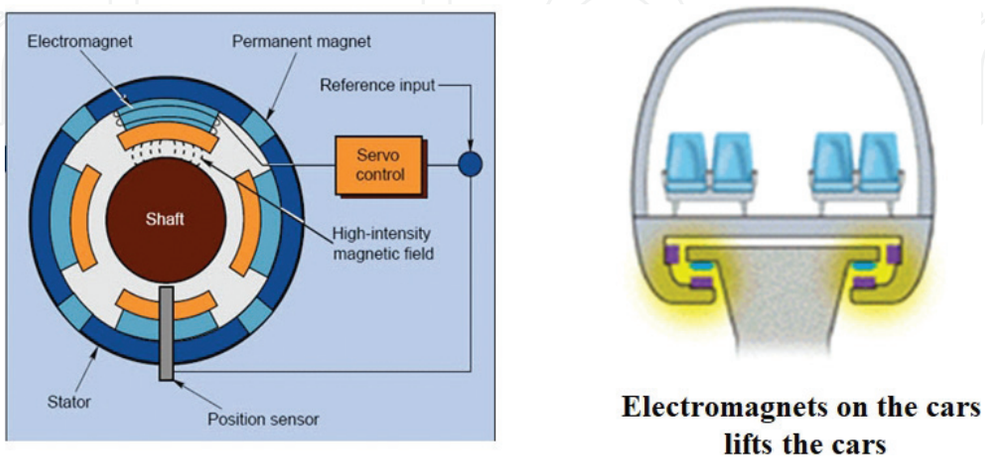

Figure 1. Applications of magnetic levitation.

http://dx.doi.org/10.5772/intechopen.75088

Most notable advances achieved in diesel engines resulted directly from superior fuel injection system designs [9].

Unlike its spark-ignited engine counterpart, the diesel fuel injection system delivers fuel under extremely high injection pressures (e.g., around 2000 [bar]). This means that the system component designs and materials should be selected to withstand higher stresses [10].

The actuators used in diesel fuel injection systems can be either electromagnetic (our focus) or piezoelectric [11]. A diesel fuel injection system using an electromagnetic actuator, from Bosch [12], is shown in **Figure 2**.

Nowadays, most of the fuel injection systems are electronically controlled. However, it is still not enough to deliver an accurate amount of fuel at the proper time to achieve good combustion. Additional aspects are critical to ensure proper fuel injection system performance, such as [9]:

- Fuel atomization—ensuring that fuel atomizes into very small fuel particles is a primary design objective for diesel fuel injection systems.
- Bulk mixing—while fuel atomization and complete evaporation of fuel are critical, ensuring that the evaporated fuel has sufficient oxygen during combustion is equally important to ensure optimum engine performance.
- Air utilization—effective utilization of the air in the combustion chamber is closely tied to bulk mixing and can be accomplished by dividing the total injected fuel into a number of jets.

While conventional fuel injection systems employ a single injection event for every engine cycle, newer systems can use multiple injection events [12].

Using multiple injections—during every engine cycle—higher engine performance and lower engine noise can be achieved. However, the injector lifetime might be reduced, and therefore advanced control algorithms as well as malfunction detection and fault isolation algorithms can be applied (see next sections).

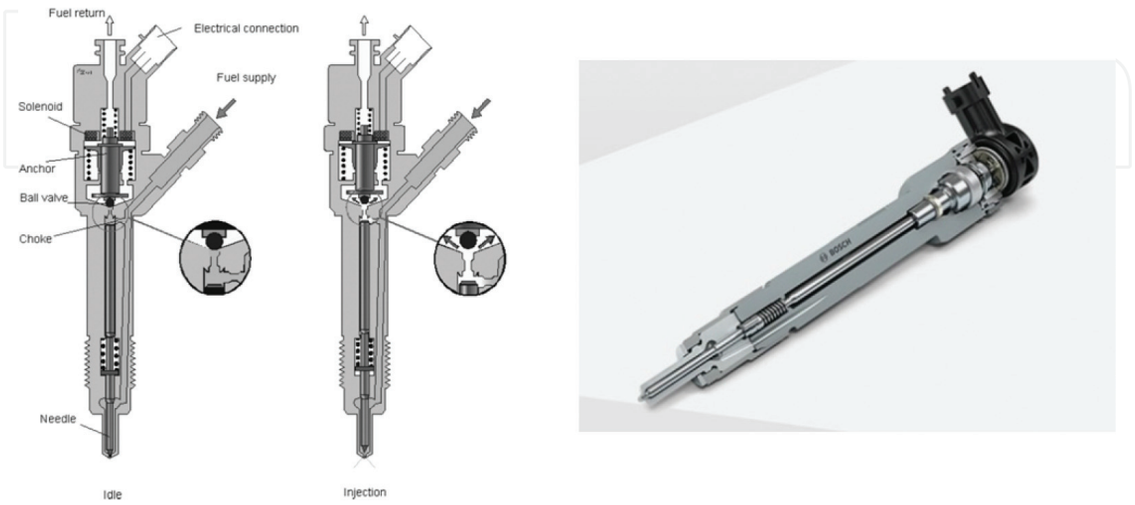

Figure 2. Diesel fuel injection system from Bosch.

Another relevant application is the electromechanical valve actuators used in automotive engines, to achieve variable valve timing (VVT). With VVT, larger valve overlap, valve lift, duration, and timing adjustments can be achieved depending on engine speed, load, and temperature.

Variable valve timing leads to improved fuel economy and lower emissions by decoupling the valve timing from the piston motion [13]. This is especially valid in case of advanced combustion technologies, as described in [14, 15].

However, the moving components of the valve actuators create unnecessary wear and excessive noise. The armature landing speed shall be kept, e.g., under 0.1 [m/s]; otherwise, they are excessively loud and are damaging to the actuator and engine valve.

Whenever high-performance and high-accuracy control is required, the electromagnetic actuator is driven by a half H-bridge (see **Figure 3**), which might be equipped optionally with a current sensing resistor R_{SENSE}.

Typical voltage and current waveforms as well as the switching order of the commutation elements T_1 and T_2 are shown in **Figure 3**.

After the electromagnetic armature is pulled up, the actuator current is reduced, and the commutation elements are controlled via pulse-width modulation (PWM).

During armature movement, due to the induced electromotive force (e.m.f.), a small current dip as well as a small current peak might be observed (see **Figure 3**).

The duty factor of the actuator—specified on the data sheet—is defined as

$$Duty[\%] = \frac{T_{ON}}{T_{ON} + T_{OFF}} 100[\%] \tag{1}$$

In practice, exceeding this value might shorten significantly the lifetime of the actuator.

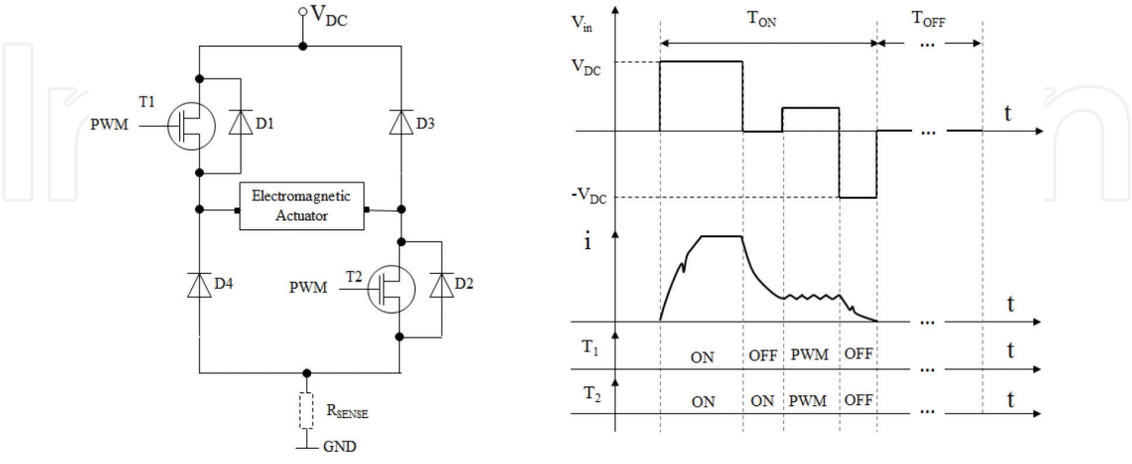

Figure 3. Electromagnetic actuator driven by a half H-bridge.

http://dx.doi.org/10.5772/intechopen.75088

2. Mathematical modeling

The mathematical model of the electromagnetic actuator is described by the voltage equation and by the motion equation.

The voltage equation is

$$v_{in} = Ri + \frac{\partial \Psi}{\partial i}\frac{di}{dt} + \frac{\partial \Psi}{\partial z}\frac{dz}{dt} \tag{2}$$

where v_{in} is the applied voltage, i is the armature current, Ψ is the armature flux, z is the armature position, and R is the electrical resistance of the coil.

If we note with $v = \dot{z}$, the armature speed and then the equation of the motion can be written as

$$m\ddot{z} = F_S - F_m \tag{3}$$

where m is the moving mass, F_m is the electromagnetic force, and F_S is the spring force. Since the armature displacement often is very short, the spring force can be considered constant. In case of magnetic levitation, the spring force is replaced by the weight of the moving mass.

The electromagnetic force can be expressed based on the electromagnetic co-energy W_{co}:

$$W_{co} = \int_0^i \Psi di \tag{4}$$

$$F_m = -\left.\frac{\partial W_{co}}{\partial z}\right|_{i=ct} \tag{5}$$

Then, we can also write

$$F_m = -\int_0^i \frac{\partial \Psi}{\partial z} di \tag{6}$$

The $\Psi = \Psi(i, z)$ and $F_m = F_m(i, z)$ static characteristics can be measured. The flux-linkage characteristic is derived by integration (very often the current decay test is used). Thus, the flux linkage for one fixed position z is calculated by

$$\Psi(i, z) = \int_0^\infty [v_{in}(t) - R \cdot i(t)]dt \tag{7}$$

where at $t = 0$ and the following conditions hold: $v_{in} = 0$, $i \neq 0$, and $di/dt = 0$.

Although the model does not take into account the effect of eddy currents, the numerical model can be very accurate and might be written formally into a nonlinear form:

$$\dot{x} = f(x) + \sum_{i=1}^{m} g(x)u \tag{8}$$

where $x = [i \ v \ z]^T$ represents the state of the nonlinear system, $u = [v_{in} \ F_S]^T$ is the input vector, and $f(x)$ and $g(x)$ are nonlinear functions of the state x. The output vector y is

$$y = h(x) \tag{9}$$

where $h(x)$ in the most general case is a nonlinear function.

Finally, in the aim to illustrate our investigations, let us consider an electromagnetic actuator with parameters (catalog data) mentioned in **Table 1** [16].

2.1. Nonlinear model and piecewise linearization

The mathematical model described above is too general and is difficult to handle in analytical form. Therefore, we define an analytical model set, which describes the flux-linkage characteristic as

$$\Psi(i,z) = \Psi_{max}\left[1 - \exp\left(-\frac{i}{c_1 + c_2 z}\right)\right] \tag{10}$$

where the parameters of the model set are Ψ_{max}, c_1, and c_2.

Furthermore, the partial derivatives of the flux-linkage are

$$\frac{\partial \Psi}{\partial i} = \frac{\Psi_{max}}{c_1 + c_2 z}\exp\left(-\frac{i}{c_1 + c_2 z}\right) \tag{11}$$

$$\frac{\partial \Psi}{\partial z} = -\frac{\Psi_{max} \cdot c_2 \cdot i}{(c_1 + c_2 z)^2}\exp\left(-\frac{i}{c_1 + c_2 z}\right) \tag{12}$$

The approach presented in this section is reproduced from [17].

Type	**Solenoid valve**
Stroke length	10 [mm]
Operating voltage	24 [V] d.c.
Maximum current	0.6 [A]
Resistance	40 [Ω]
Inductance	0.35–1.1 [H]
Number of turns	2240

Table 1. The solenoid parameters.

http://dx.doi.org/10.5772/intechopen.75088

If we approximate the exponential term by Taylor series, we have

$$\exp\left(-\frac{i}{c_1+c_2z}\right)\approx 1-\frac{i}{c_1+c_2z}+\frac{i^2}{2(c_1+c_2z)^2} \tag{13}$$

Thus, the magnetic force—based on the analytical model—can be expressed as

$$F_m\approx\frac{\Psi_{max}\cdot c_2\cdot i^2}{(c_1+c_2z)^2}\left[\frac{1}{2}-\frac{i}{3(c_1+c_2z)}+\frac{i^2}{8(c_1+c_2z)^2}\right] \tag{14}$$

The model set above is validated against the measured static (flux and force) characteristics. The "dots" in **Figure 4** represent the measured data, and the solid lines represent the calculated model using the above model set, with $\Psi_{max}=0.45[Wb]$, $c_1=0.4[A]$, and $c_2=0.375\cdot 10^3[A/m]$. The above parameters are derived using nonlinear least squares, fitting the measured data (obtained using the current decay test and force measurements) with the analytical model.

Next, let us introduce the following notations, which help us to rewrite the model in a convenient form: $\chi_i=\partial\Psi/\partial i$, $\chi_z=\partial\Psi/\partial z$, and $\chi_f=F_m/i$.

Since the magnetic force F_m depends on the square of the current i^2, when the current is zero $i=0$ and then $\chi_f=0$, there is no division by zero in the model.

Thus, the voltage and motion equations are written as

$$\frac{di}{dt}=-\frac{R}{\chi_i}\cdot i-\frac{\chi_z}{\chi_i}\cdot v+\frac{1}{\chi_i}v_{in} \tag{15}$$

$$\frac{dz}{dt}=v \tag{16}$$

$$\frac{dv}{dt}=-\frac{\chi_f}{m}\cdot i-\frac{k}{m}\cdot z+\frac{1}{m}F_S(0) \tag{17}$$

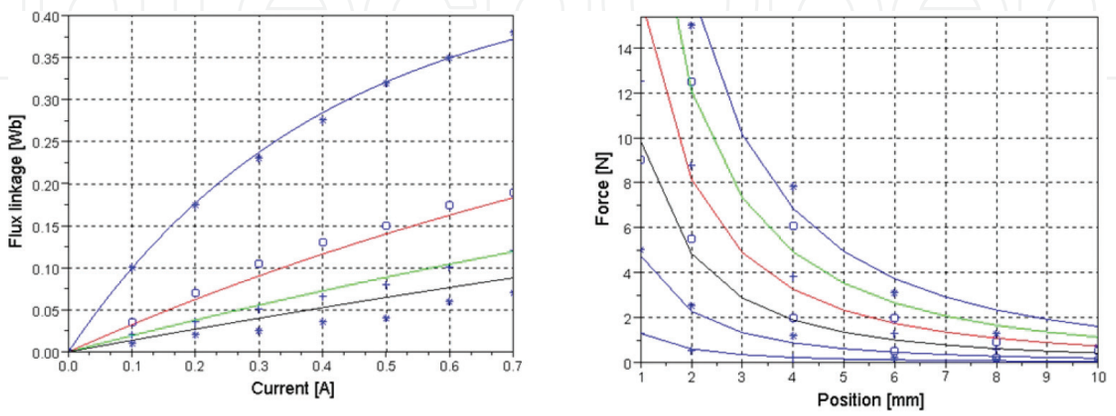

Figure 4. Flux and force characteristics.

Finally, using a piecewise approximation, the system can be written in state-space form as

$$\begin{aligned} \dot{x} &= A(i,z) \cdot x + B(i,z) \cdot u \\ y &= C \cdot x \end{aligned} \tag{18}$$

where $x = [i \;\; z \;\; v]^T$ is the state-space vector, $u = [v_{in} \;\; F_S(0)]^T$ is the input vector, y is the output vector, the $A(i,z)$ and $B(i,z)$ are current and position dependent matrices and $C = [1 \;\; 1 \;\; 0]$ if the armature current and position are sensed. We remark, that in practice sensing the armature speed and/or positions with sensor(s) might be expensive solution. Therefore, often only the armature current can be sensed in a cost-effective manner.

The terms $A(i,z)$ can be written as

$$A(i,z) = \begin{bmatrix} -R/\chi_i & 0 & -\chi_z/\chi_i \\ 0 & 0 & 1 \\ -\chi_f/m & -k/m & 0 \end{bmatrix} \tag{19}$$

where

$$-\frac{\chi_z}{\chi_i} = \frac{c_2 \cdot i}{c_1 + c_2 z} \tag{20}$$

The term $B(i,z)$ can be written as

$$B(i,z) = \begin{bmatrix} 1/\chi_i & 0 \\ 0 & 0 \\ 0 & 1/m \end{bmatrix} \tag{21}$$

where

$$\frac{1}{\chi_i} \approx \frac{2(c_1 + c_2 z)^2 + 2i(c_1 + c_2 z) + i^2}{2 \cdot \Psi_{max} \cdot (c_1 + c_2 z)} \tag{22}$$

or a coarser approximation will be

$$\frac{1}{\chi_i} \approx \frac{c_1 + c_2 z + i}{\Psi_{max}} \tag{23}$$

Last but not least, the armature movement is subject to the following constraints:

$$v(t) = \begin{cases} 0 & if \quad z \geq z_{max} \quad and \quad F_s - F_m \geq 0 \\ 0 & if \quad z \leq 0 \quad and \quad F_s - F_m \leq 0 \end{cases} \tag{24}$$

as well as $z_{min} \leq z(t) \leq z_{max}$, where z_{min} and z_{max} are the minimum and maximum displacements of the armature.

http://dx.doi.org/10.5772/intechopen.75088

2.2. Linearized mathematical model

From control engineering viewpoint—in case of some applications (e.g., magnetic levitation)—the piecewise linearized model might be too sophisticated. Therefore, in this section a linearized mathematical model around an operating point is derived [1, 18].

Let us approximate the magnetic force as

$$F_m \approx \gamma \frac{i^2}{(c_1 + c_2 z)^2} \tag{25}$$

where γ is a constant.

The equation of motion can be written as

$$M(z, \ddot{z}, i) = m\ddot{z} - F_s + \gamma \frac{i^2}{(c_1 + c_2 z)^2} = 0 \tag{26}$$

The equation above can be linearized around an operating point $p_0 = (z_0, \ddot{z}_0, i_0)$ as follows:

$$M(z, \ddot{z}, i) = M(z_0, \ddot{z}_0, i_0) + \frac{\partial M}{\partial z}\bigg|_{p_0}(z - z_0) + \frac{\partial M}{\partial \ddot{z}}\bigg|_{p_0}(\ddot{z} - \ddot{z}_0) + \frac{\partial M}{\partial i}\bigg|_{p_0}(i - i_0) \tag{27}$$

which can be further written as

$$M(z, \ddot{z}, i) = -\frac{2\gamma i_0^2}{(c_1 + c_2 z_0)^3}(z - z_0) + m(\ddot{z} - \ddot{z}_0) + \frac{2\gamma i_0}{(c_1 + c_2 z_0)^2}(i - i_0) = 0 \tag{28}$$

If we denote with $\Delta z = z - z_0$ and $\Delta i = i - i_0$, we obtain

$$-\frac{2\gamma i_0^2}{(c_1 + c_2 z_0)^3}\Delta z + m\Delta\ddot{z} + \frac{2\gamma i_0}{(c_1 + c_2 z_0)^2}\Delta i = 0 \tag{29}$$

If we divide the equation with the moving mass m and apply the Laplace transform, we obtain

$$\left(s^2 - a^2\right)\Delta z(s) + k\Delta i(s) = 0 \tag{30}$$

$$\frac{\Delta z(s)}{\Delta i(s)} = -\frac{k}{s^2 - a^2} = -\frac{k}{(s - a)(s + a)} \tag{31}$$

where k and a are varying with the equilibrium point (i_0, z_0):

$$k = \frac{2\gamma i_0}{m(c_1 + c_2 z_0)^2} \tag{32}$$

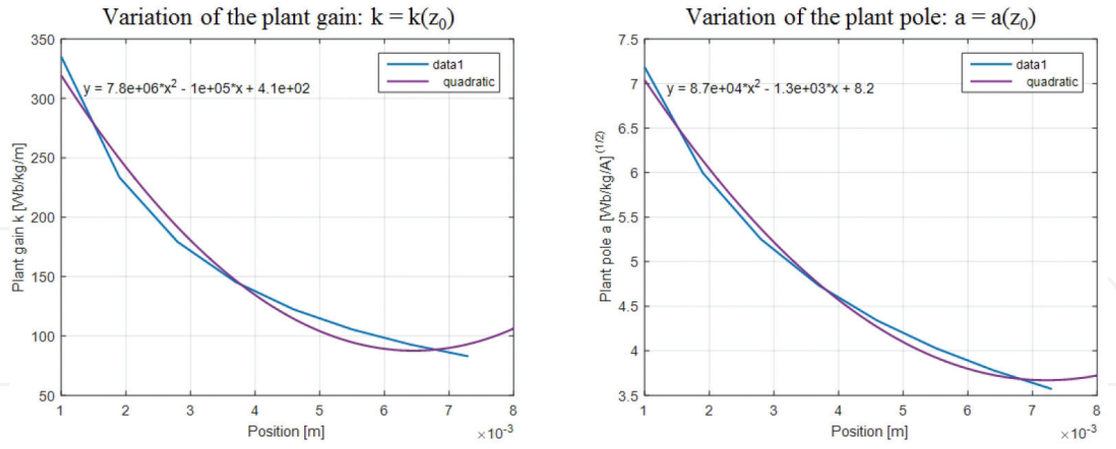

Figure 5. Plant gain and pole variation with the equilibrium position.

$$a^2 = \frac{2\gamma i_0^2}{m(c_1 + c_2 z_0)^3} \tag{33}$$

It means that a family of transfer functions are obtained and the system can be viewed as a linear parameter-varying (LPV) system.

The variation of k and a values with the equilibrium position z_0 is shown in **Figure 5** and can be well approximated by quadratic functions.

3. System identification

3.1. Clustering-based system identification

In the previous section, we have seen that using the current decay test and the nonlinear least squares method, the parameters of the mathematical model can be identified.

However, the current decay test is time-consuming, since measurements shall be performed for each grid point defined by armature current and position (i, z). Thus, the obvious question might arise: is there a faster solution to identify the parameters?

During the system identification process, we will note the system's input and output at time t by $u(t)$ and $y(t)$, respectively [19].

For single-input single-output linear systems, we can write

$$y(t) = \varphi^T(t)\theta \tag{34}$$

where θ is the parameter vector (unknown) and the φ is the recorded (known) input-output data vector:

$$\begin{aligned} \theta &= [a_1 \ldots a_n \qquad b_0 \ldots b_m]^T \\ \varphi(t) &= [-y(t-1) \ldots -y(t-n) \quad u(t) \ldots u(t-m)]^T \end{aligned} \tag{35}$$

To emphasize that the calculation of the $y(t)$ is from the past data, we will write

$$\widehat{y}(t) = \varphi^T(t)\theta \tag{36}$$

Now, suppose for a given system that we do not know the values of the parameters in θ, but we have recorded inputs and outputs over the time interval. If the input signal is persistently exciting—condition described in details in [19, 20]—then the solution can easily be computed by modern software tools.

In this section a clustering-based identification method, proposed by Ferrari-Trecate et al. (2003) is used (see [21, 22]), where the plant is assumed to be described by piecewise linear models having s sub-models, such as

$$y(t) = \begin{cases} \varphi^T(t)\theta_1 + w(t), & if \quad \varphi^T(t) \in C_1 \\ \vdots & \\ \varphi^T(t)\theta_s + w(t), & if \quad \varphi^T(t) \in C_1 \end{cases} \tag{37}$$

where $w(t)$ is white noise, θ_i $i = 1, \ldots, s$ are the parameter vectors, $\varphi(t)$ is a regression vector, and n is the order of the piecewise ARX (PWARX) model.

It is assumed that the order of each sub-model is the same, and u(t) and y(t) are the input and output, respectively.

Furthermore, it is assumed that $C_{i=1}^s$ are polytopic and they satisfy the well-posed condition: $\cup_{i=1}^s C_i = C$, $C_i \cap \ C_j = \varnothing$, and $\forall i \neq j$.

An important phase of the system identification experiment is input signal design. In case of nonlinear systems, a multilevel random signal is often used [23, 24], and a bi-level pseudorandom binary signal (PRBS) is not suitable for nonlinear systems.

The generation of the multilevel random signal—using shift registers—is done according to [25]. **Figure 6** shows a five-level random signal with maximal length, using four-shift registers with coefficients $a_1 = 1, a_2 = -1, a_3 = 1, a_4 = -2$ [25].

This input signal is applied—when the armature is fixed—in order to identify the dynamic inductance denoted by χ_i and the electrical resistance R. The output signal—armature current —when the multilevel random signal is applied is shown in **Figure 6**.

Next, the voltage equation is written in discrete form at the time moment $t = t(k)$:

$$i(k) = \frac{T_S}{\chi_i + RT_S} v_{in}(k) + \frac{\chi_i}{\chi_i + RT_S} i(k-1) \tag{38}$$

where T_S is the sampling time.

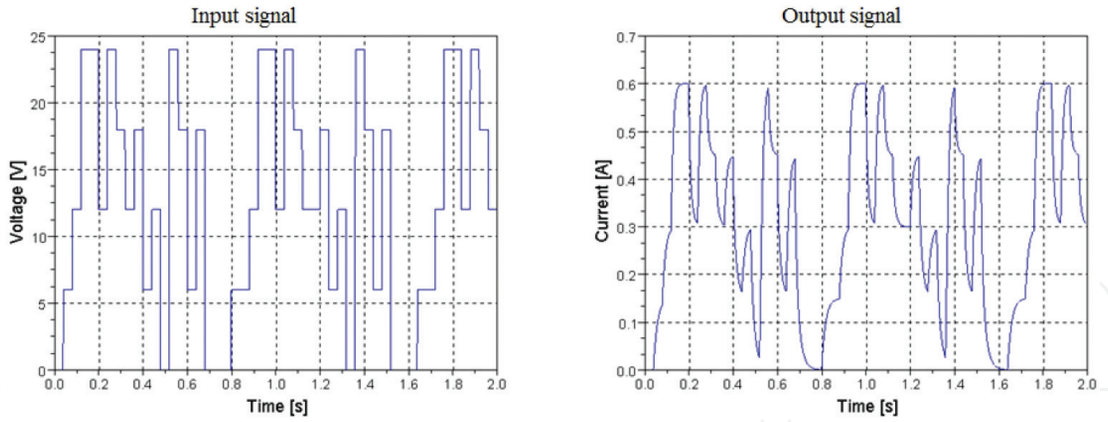

Figure 6. Multilevel random input and corresponding output signal.

The equation above defines the regression space (see also references [21, 22]) having in this case two axis, defined by $i(k-1)$ and $v_{in}(k)$. The data collected during the system identification experiment is shown in the regression space in **Figure 7**.

The regression space is clustered in five different regions for $i = 0.1, \ldots, 0.5[A]$, and the parameters are identified for each case using the least squares method. In each defined cluster, we assume that χ_i is constant, and basically we use a piecewise linear approximation of χ_i.

The system identification experiments are repeated around different positions, when the armature is fixed; thus, the function $\widehat{\chi}_i = \widehat{\chi}_i(i, z)$ can be estimated.

Now, using the nonlinear least squares, we can minimize the J objective function:

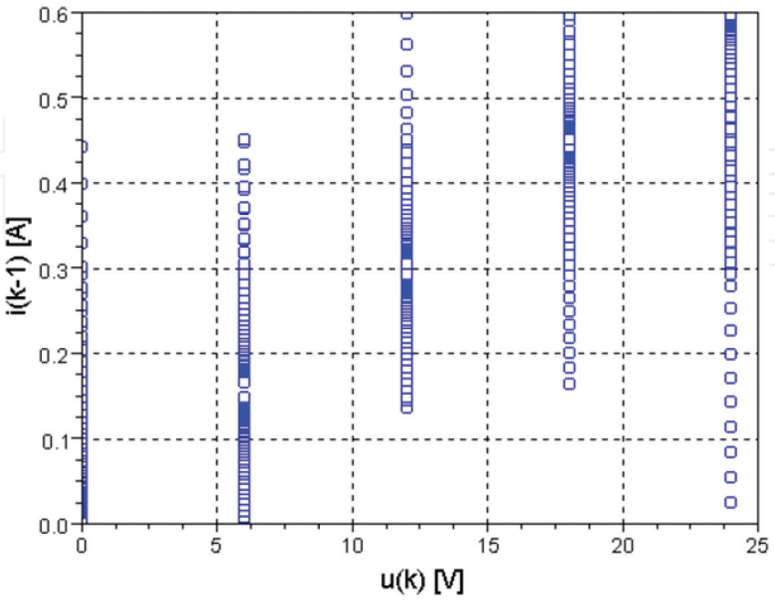

Figure 7. Regression space—Clustering-based identification.

http://dx.doi.org/10.5772/intechopen.75088

$$J = \min(\chi_i(i,z) - \widehat{\chi}_i(i,z))^2 \tag{39}$$

and we can find out the estimated parameters of the model $\widehat{\Psi}_{max} = 0.437[Wb]$, $\widehat{c_1} = 0.37[A]$, and $\widehat{c_2} = 0.36 \cdot 10^3[A/m]$. Values, which are in good accordance with the values, are found via the current decay test.

Having the $\chi_i = \chi_i(i,z)$ function identified, the parameters of the model set, namely, Ψ_{max}, c_1, and c_2, are found.

This identification is repeated only around different positions z, when the armature is fixed and thus is much faster than identifying $\Psi = \Psi(i,z)$ around different current and position values using the current decay test.

3.2. Identification under closed-loop

In practice, it might be the case that the system is open-loop unstable; thus, system identification experiments have to be performed under closed-loop (for more details see [26, 27]).

Closed-loop identification is a very challenging task. Due to the presence of feedback loop, the input signal might not be persistently exciting. In the aim to achieve a persistent excitation of the system, it is recommended in [19] to switch between different simple controller structures.

First, the system shall be stabilized under feedback around an equilibrium position, as shown in **Figure 8**; details about the controller design $K(s)$ are described in the next section.

Under closed loop, the reference input (armature position) is disturbed by a persistently exciting input signal (i.e., pseudorandom binary signal)—as shown in **Figure 9**, and three linear transfer functions are identified, which are defined as

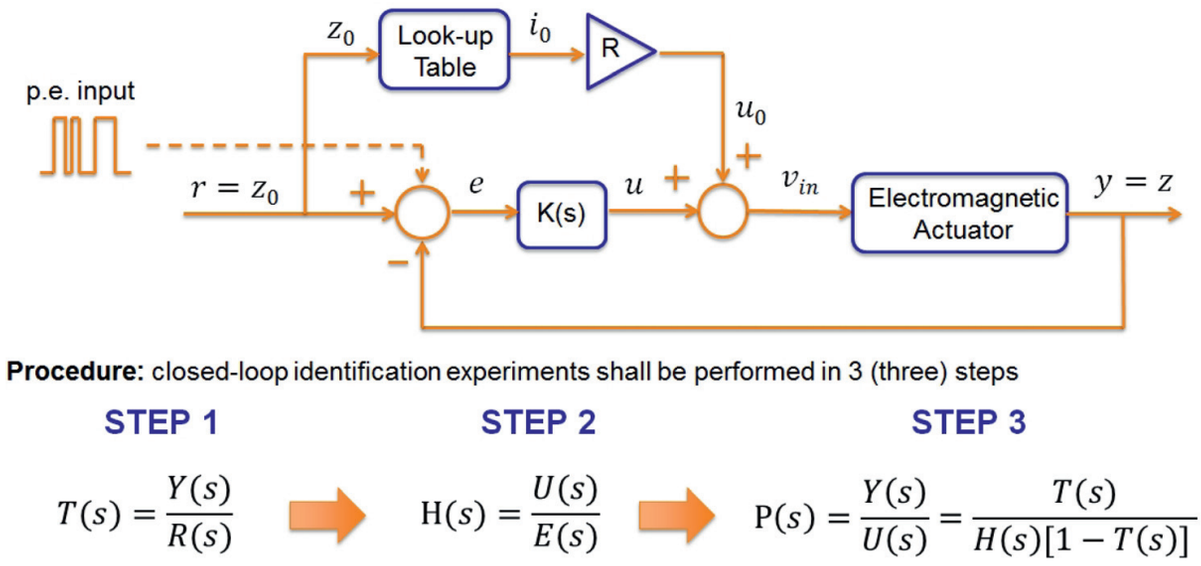

Figure 8. Closed-loop system identification.

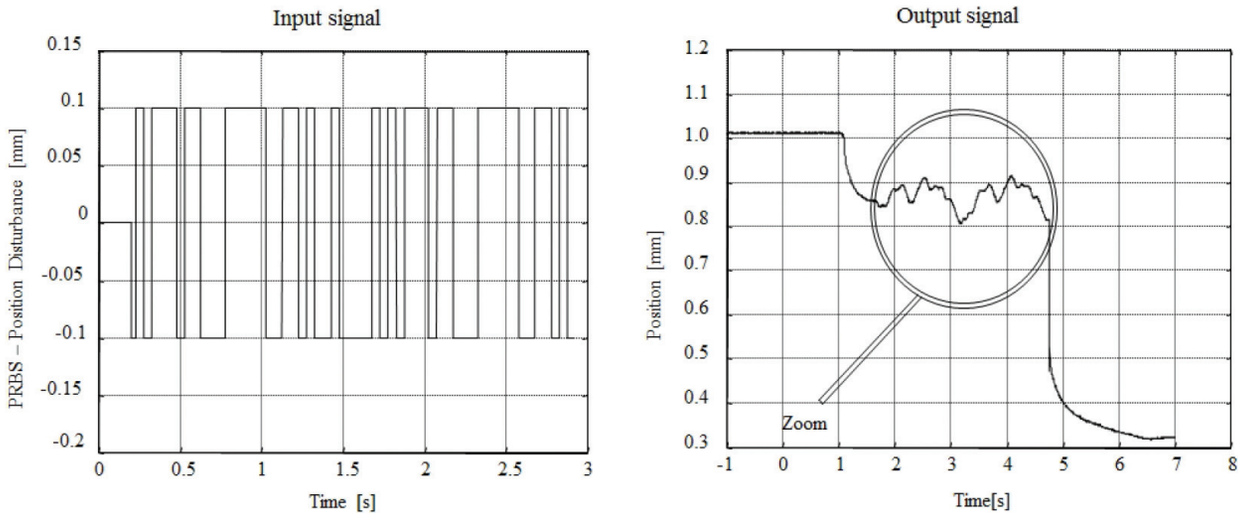

Figure 9. Input and output signal used to identify $T(s)$.

$$T(s) = \frac{Y(s)}{R(s)} = \frac{P(s)K(s)}{1 + P(s)K(s)} \tag{40}$$

$$H(s) = \frac{U(s)}{E(s)} = \frac{K(s)}{1 + P(s)K(s)} \tag{41}$$

$$P(s) = \frac{Y(s)}{U(s)} = \frac{T(s)}{H(s)(1 - T(s))} \tag{42}$$

where we used the well-known identity $S(s) + T(s) = 1$:

$$S(s) = \frac{E(s)}{R(s)} = 1 - T(s) \tag{43}$$

The procedure can be repeated around different equilibrium positions; thus, a family of transfer functions can be obtained.

4. Control of electromagnetic actuators

Let us start with the easier case: the moving armature is controlled around an equilibrium position—magnetic bearings and magnetically levitated high-speed trains are typical applications.

The linearized mathematical model, around an equilibrium position, can be written as

$$P(s) = \frac{\Delta z(s)}{\Delta i(s)} = -\frac{k}{(s-a)(s+a)} \tag{44}$$

where k and a are strictly positive values, varying with the equilibrium point (i_0, z_0).

In this section, we are looking for a linear controller, which can stabilize the plant and can fulfill performance and robustness requirements [18].

4.1. PD controller

A very simple PD controller, which can stabilize the plant, is

$$K(s) = -k_D(s + a) \tag{45}$$

The closed-loop transfer function shows that

$$T(s) = \frac{kk_D}{s + kk_D - a} \tag{46}$$

The system is stable if $kk_D > a$; however, the steady-state error might be significant, since the controller gain k_D cannot be made arbitrarily large.

4.2. PI controller

The next option is to consider a PI controller such as

$$K(s) = -k_{PI}\frac{s + a}{s} \tag{47}$$

In this case, the closed-loop transfer function becomes

$$T(s) = \frac{kk_{PI}}{s^2 - as + kk_{PI}} \tag{48}$$

Since a is a positive value, we observe that the PI controller cannot stabilize the plant $P(s)$.

4.3. PID controller

Let us consider a PID controller—having a single tuning parameter K_{PID}—in the form

$$K(s) = -k_{PID}\frac{(s + a)^2}{s} \tag{49}$$

The block diagram of the control system is shown in **Figure 10**.

The closed-loop transfer function is

$$T(s) = \frac{kk_{PID}(s + a)}{s^2 + (kk_{PID} - a)s + kk_{PID}a} \tag{50}$$

The closed-loop transfer function has a zero at $s = -a$, which might affect the system response (large overshoot), which can be canceled with a prefilter $K_{PRE}(s) = a/(s + a)$.

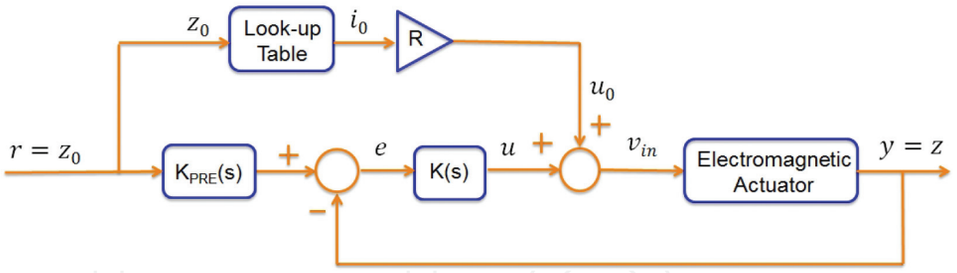

Figure 10. The block diagram of the control system.

Then, the closed-loop transfer function becomes

$$T(s) = \frac{kk_{PID}a}{s^2 + (kk_{PID} - a)s + kk_{PID}a} \tag{51}$$

Next, based on performance and robustness specifications, we would like to find a suitable value for the controller gain K_{PID}. Usually, performance specifications are given in terms of settling time T_{set} and percent of overshoot $P.O.$

For a second-order system

$$T(s) = \frac{\omega_n^2}{s^2 + 2\tau\omega_n s + \omega_n^2} \tag{52}$$

where ω_n is the natural frequency and the τ is the damping factor; we have $T_{set} \approx 4/(\tau\omega_n)$ and $P.O. = 100 \cdot e^{-\tau\pi/\sqrt{1-\tau}}$.

Since we have only one tuning parameter K_{PID}, the performance specifications are given only in terms of settling time $T_{set} = 1.25[s]$. Therefore, the PID controller gain can be calculated as

$$kk_{PID} - a = 2\tau\omega_n \approx \frac{8}{T_{set}} \tag{53}$$

Thus, we obtain

$$k_{PID} = \frac{8 + aT_{set}}{kT_{set}} \tag{54}$$

Next, the stability and robustness in a classical framework can be assessed. We calculate the gain and phase margins, obtaining $G_m = 0.47[m/A]$ and $P_m = 37[\text{deg}]$ for the equilibrium position $z_0 = 3 \cdot 10^{-3}[m]$.

4.4. Gain-scheduled controller

We have seen that the actuator can be stabilized around, and equilibrium point and performance and robustness can be guaranteed.

However, we observed that the plant parameters k and a are varying with the operating point (i_0, z_0); thus, for good performance and robustness, the controller should take into account that the plant parameters are varying.

A survey of linear parameter-varying control applications can be found in [28], and control applications validated by experiments are presented in [27, 29] for actuators and for medical X-ray systems in [30]. High-accuracy mathematical modeling and a linear parameter-varying observer for fault detection and fault isolation are presented in [17].

We can design a linear parameter-varying controller having the form

$$K(s, z_0) = k_{PID}(z_0) \frac{(s + a(z_0))^2}{s} \tag{55}$$

where both the controller gain and controller zero are dependent on the equilibrium position.

Finally, stability and robustness (quadratic stability) of such a control system can be analyzed using modern software tools, and details are described in [27].

If a simpler approach is preferred, a gain-scheduled controller might be a good choice, which is easier to implement in real time, and its stability and robustness are easier to analyze.

Since perfect cancelation of the varying plant pole at $s = -a$ with a fixed controller zero is not possible, we choose to place the controller fixed zero left to the varying poles, such as $z = -a_{max}$. Then, the gain-scheduled controller can be written as

$$K(s, z_0) = k_{PID}(z_0) \frac{(s + a_{max})^2}{s} \tag{56}$$

where the only one tuning parameter is controller gain $K_{PID}(z_0)$, defined as

$$k_{PID}(z_0) = \frac{8 + a(z_0) T_{set}}{k(z_0) T_{set}} \tag{57}$$

where the variation of the values $k = k(z_0)$ and $a = a(z_0)$ were shown already in **Figure 5**.

Next, the gain and phase margins are calculated for different equilibrium positions z_0 and shown in **Figure 11**. We can observe that—due to the gain-scheduled controller—the gain and phase margins do not change significantly with the equilibrium position, and such a robustness is difficult to achieve with a single controller, having fixed parameters.

The system response using the gain-scheduled controller is investigated, considering the following two cases:

- The moving armature is controlled around an equilibrium position, and the set point (reference position) is changed $\Delta z_0 = 1[mm]$ (see **Figure 12**, left plot). The control system —including the prefilter—exhibits approximately $P.O. \approx 25\%$ overshoot and settling time $T_{set} = 1.5[s]$.

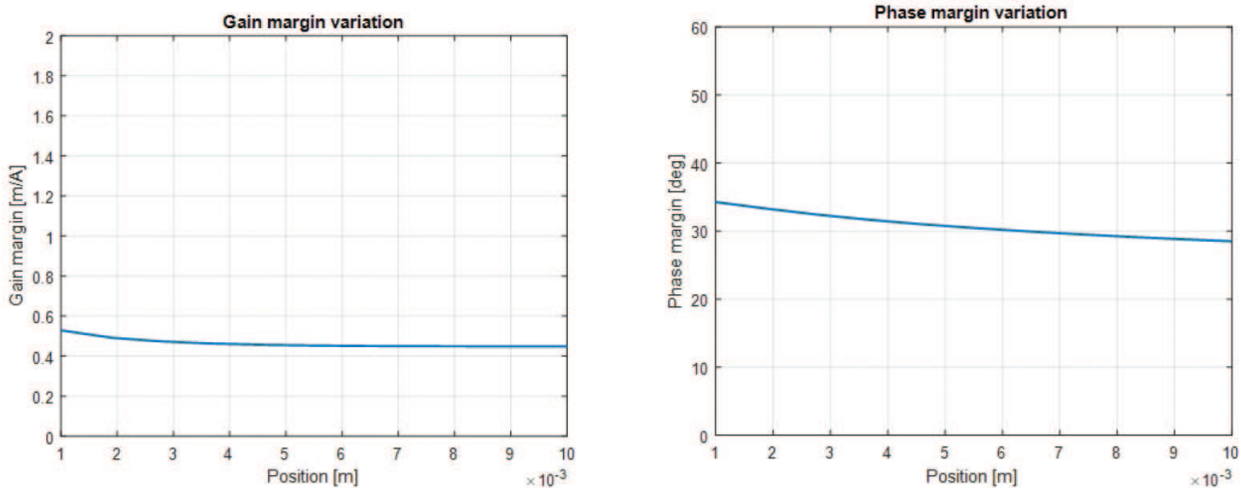

Figure 11. Gain and phase margin variation with z_0.

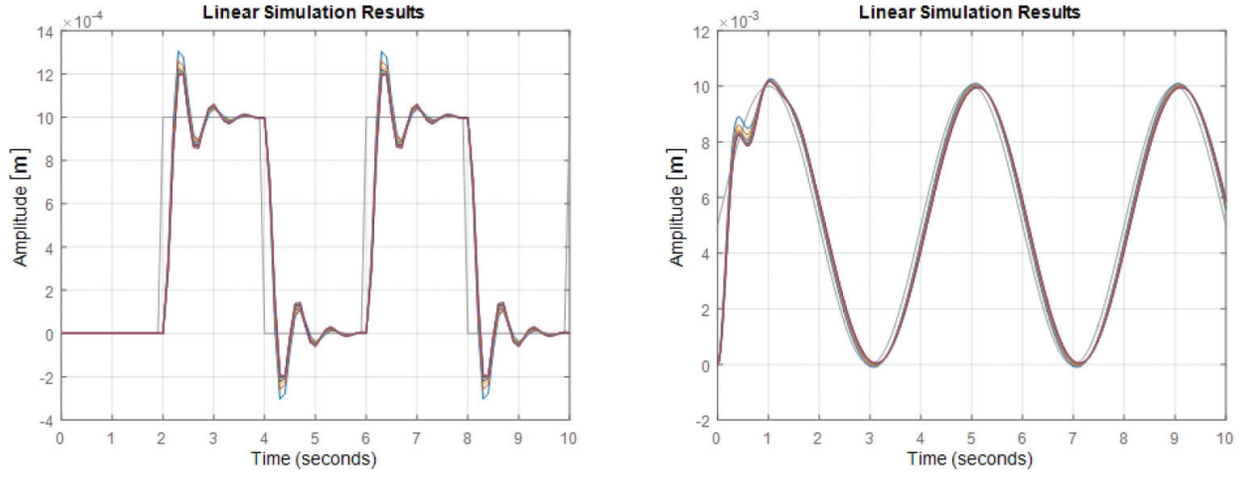

Figure 12. System response with the gain-scheduled controller.

- The moving armature is controlled between the two extreme positions, armature open and armature close, $\Delta z_0 = 10[mm]$ (see **Figure 12**, right plot). In this case the main goal is to achieve so-called soft landing of the moving armature to reduce wear and noise.

It is important to highlight that controller design is made based on the linearized plant, but validation of the controller in simulations or during hardware-in-the-loop (HIL) experiments shall be done using the nonlinear plant model.

During our control design investigations, we considered that the armature position can be measured. In practice, there are applications, where the armature position cannot be measured in a cost-effective way.

Therefore, we remark that controlling the moving armature without measuring the armature position (e.g., measuring only the current) remains a challenging research topic, which exceeds the goals and the limits of this chapter.

5. Conclusions

This chapter dealt with mathematical modeling, system identification, and control of electromagnetic actuators. Actuators are often used in industrial applications such as magnetic levitation, electromagnetic bearings, as well as in fuel injectors in the automotive industry.

After a detailed mathematical model was presented, two different parameter identification techniques were described. The first one is based on the classical current decay test, and the second one is a clustering-based system identification approach. Since the actuator is open-loop unstable, the main steps of system identification of the actuators under closed-loop control were presented.

Finally, very simple and easy-to-apply control strategies were discussed, when the armature is controlled around a fixed equilibrium position (PID controller) as well as when the armature is controlled between two extreme positions, armature open and armature closed (gain-scheduled PID controller).

Author details

Alexandru Forrai

Address all correspondence to: alexandru.forrai@tno.nl

TNO, Helmond, The Netherlands

References

[1] Bittar A, Sales RM. H_2 and H_∞ control for MagLev vehicles. IEEE Control Systems. 1998; **18**(4):18-25

[2] Lindlau JD, Knospe CR. Feedback linearization of an active magnetic bearing with voltage control. IEEE Transaction on Control Systems Technology. 2002;**10**(1):21-31

[3] Li L, Shinshi T, Shimokohbe A. Asymptotically exact linearizations for active magnetic bearing actuators in voltage control configuration. IEEE Transaction on Control Systems Technology. 2003;**11**(2):185-195

[4] Fittro RL, Knospe CR. Rotor compliance minimization via μ-control of active magnetic bearings. IEEE Transaction on Control Systems Technology. 2002;**10**(2):238-250

[5] Duan G-R, Howe D. Robust magnetic bearing control via eigenstructure assignment dynamical compensation. IEEE Transaction on Control Systems Technology. 2003;**11**(2): 204-215

[6] http://mechanicstips.blogspot.nl/2015/06/

[7] http://www.personal.psu.edu/cjm5/

[8] Yaghoubi H, Barazi N, Aoliaei MR: Maglev. In: Infrastructure design, signalling and security in railway. InTechOpen, pp. 123-176

[9] https://www.dieselnet.com/tech/diesel-fi.php

[10] Robert Bosch GmbH. Diesel-Engine Management. Plochingen: Bosch; 2004

[11] Breitbach H. Fuel Injection Systems Overview. Delphi Corporation; 2002

[12] http://www.bosch-mobility-solutions.com/en

[13] Hoffmann W, Peterson K, Stefanopoulou A. Iterative learning control for soft landing of electromechanical valve actuator in camless engines. IEEE Transaction on Control Systems Technology. 2003;**11**(2):174-184

[14] Doosje E, Willems F, Baert R. Experimental demonstration of RCCI in heavy-duty engines using diesel and natural gas. SAE Technical Paper 2014-01-1318; 2014. DOI: 10.4271/2014-01-1318

[15] Mikulski M, Balakrishnan PR, Doosje E, Bekdemir C. Variable valve actuation strategies for better efficiency, load range, and thermal management in an RCCI engine. SAE Technical Paper 2018-01-0254; 2018 (to be published)

[16] Rahman MF, Cheung NC, Lim KW. Modelling of a nonlinear solenoid towards the development of a proportional actuator. Vol 1. In: Proceedings of the 5th International Conference on Modelling and Simulation of Electrical Machines, Convertors, and Systems, ELECTRIMACS'96; Saint Nazaire. September 17–19, 1996; pp. 121-128

[17] Forrai A. System identification and fault diagnosis of an electromagnetic actuator. IEEE Transaction on Control Systems Technology. 2016;**25**(3):1028-1035

[18] Folea S, Muresan CI, De Keyser R, Ionescu CM. Theoretical analysis and experimental validation of a simplified fractional order controller for a magnetic levitation system. IEEE Transaction on Control Systems Technology. 2016;**24**(2):756-763

[19] Ljung L. System Identification – Theory for the User. New York: Prentice-Hall; 1987

[20] Forrai A. Embedded Control System Design – A Model Based Approach. Berlin/Heidelberg: Springer; 2012

[21] Ferrari-Trecate G, Muselli M, Liberati D, Morari M. A clustering techniques for the identification of piecewise affine systems. Automatica. 2003;**39**(2):205-217

[22] Hirata M, Noguchi S, Adachi S. A hybrid modeling method for precise positioning systems. In: Proceeding of the 17th World Congress. Seoul: The International Federation of Automatic Control; 2008. pp. 1797-1802

[23] Barker HA, Rivera DE, Tan AH, Godfrey KR. Perturbation signal design. In: 14th IFAC Symposium on System Identification; 2006. pp. 1121-1126

[24] Ljung L. Approaches to identification of nonlinear systems. In: Proceedings of 29th Chinese Control Conference, Beijing; 2010

[25] Haber R, Keviczky L. Nonlinear System Identification. Berlin: Springer; 1999

[26] Forrai A, Ueda T, Yumura T. Asymptotically exact linearization and robust control of an electromagnetic actuator. Vol. II. In: Proceedings of PCIM'04 Conference, Nuremberg; 2004. pp. 788-793

[27] Forrai A, Ueda T, Yumura T. Electromagnetic actuator control: A linear parameter-varying (LPV) approach. IEEE Transaction on Industrial Electronics. 2007;**54**(3):1430-1441

[28] Hoffmann C, Werner H. A survey of linear parameter-varying control applications validated by experiments or high-fidelity simulations. IEEE Transaction on Control Systems Technology. 2015;**23**(2):416-433

[29] Kahveci NE, Kolmanovsky IV. Control design for electromagnetic actuators based on backstepping and landing reference governor. In: 5th IFAC Symposium on Mechatronic Systems; 2010. pp. 393-398

[30] van der R, van der Maas A, Voorhoeve R, Oomen T. Accurate FRF identification of LPV systems: nD-LPM with application to a medical X-ray system. IEEE Transaction on Control Systems Technology. 2017;**25**(5):1724-1735

IntechOpen